

Overview of Recent Results from Alcator C-Mod including Applications to ITER Scenarios

E. S. Marmor and the Alcator C-Mod Team

MIT Plasma Science and Fusion Center, Cambridge MA 02139 USA

E-mail contact of main author: marmor@psfc.mit.edu

Abstract: We have significantly extended the I-mode regime, which exhibits decoupled particle and energy transport in the pedestal, to high power and plasma performance. I-mode yields a strong edge ion and electron temperature barrier, excellent energy confinement ($H_{\text{ITER-98}}$ up to 1.3), low collisionality, with L-mode like density and impurity transport, and no build-up of a density pedestal. The decoupling of the density and temperature pedestals allows ∇T to be identified as the driving term for spontaneous rotation (not ∇P or ∇n). The efficiency of ICRF induced flow drive on C-Mod depends strongly on He^3 concentration in the D(He^3) mode conversion regime, with driven core toroidal rotation up to 110 km/s ($M \sim 0.3$). Lower Hybrid Current Drive (LHCD) experiments have shown efficient propagation, damping and current drive, up to plasma electron densities of about $1 \times 10^{20} \text{ m}^{-3}$, in good agreement with results from state of the art simulation codes. At higher densities, the efficiency drops off more rapidly than expected from modeling, and mechanisms of anomalous absorption in the edge plasma are under investigation. Long-pulse non-inductive scenarios for ITER anticipate the addition of LHCD upgrades to the facility, and assume efficient off-axis current drive at about the density where these effects appear on C-Mod. Runaway acceleration during mitigated disruptions is studied using LHCD to provide a seed of epithermal electrons; results show a strong dependence on plasma shape, with significant production of runaways after the thermal quench for low elongation plasmas. Studies of hydrogen isotope retention with high-Z plasma facing components, another critical ITER issue, reveal that single discharge retention in the tokamak can be substantially higher than is seen in low-flux laboratory experiments. Plasma damage to the materials plays a significant role in creating sites for retention. Recent experiments have also revealed that relatively low energy density disruptions are effective in removing stored deuterium from the metallic surfaces, through plasma heating, as opposed to radiation; extrapolations indicate this approach could be applicable on ITER. Using low-Z impurity seeding, we have demonstrated that it is possible to reduce divertor power loads to levels that meet ITER operational requirements, while maintaining sufficient P_{net} for $H_{98} \geq 1$.

1. Introduction

Alcator C-Mod [1.1] combines high magnetic field, advanced shaping and divertor configurations, and the ability to operate with solid all-metal plasma-facing components. Because of its relatively compact size, C-Mod accesses regimes of extreme edge power density (1 MW/m² average through the surface of the plasma); SOL power widths are of order of a few mm, implying mid-plane parallel power flows $>1 \text{ GW/m}^2$, matching and even surpassing the design for ITER, and reaching the levels envisioned in DEMO power plants.

2. I-Mode

In addition to studying ELMy H-modes, which have intermittent pedestal regulation, and the higher collisionality EDA H-mode, which achieves stationary conditions through continuous pedestal regulation, we have significantly extended the I-mode regime [2.1], which decouples energy and particle transport in the pedestal, to high power and plasma performance. I-mode yields strong edge ion and electron temperature barriers, excellent energy confinement ($H_{\text{ITER-98}}$ up to 1.3), and low collisionality, with L-mode like particle and impurity transport and no build-up of a density pedestal. Figure 2.1 shows typical radial profiles comparing L-mode, H-mode and I-mode.

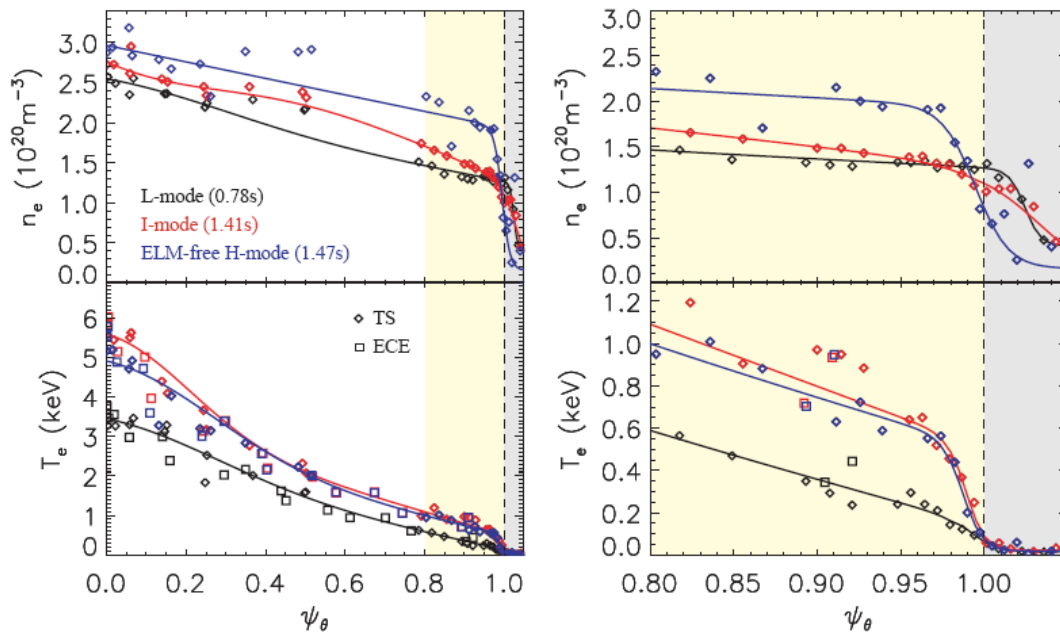


Fig.2.1. Comparisons of radial electron temperature and density profiles for typical L-, H- and I-mode discharges. The expansions on the right show the details of the pedestal, revealing the steep temperature pedestal in I-mode, while the density profile is essentially the same as for L-mode.

Figure 2.2 shows pedestal temperature and collisionality for a database of I-mode shots, along with typical EDA H-modes and L-modes for comparison. The I-mode edge is correlated with turbulence in the pedestal, higher and broader in frequency than that of the EDA QC-mode, but apparently more effective than the latter in maintaining strong particle and impurity transport with relatively little effect on energy transport, and with no need for ELMs to maintain density and impurity control (although at the highest pedestal pressures, small ELMs are observed in I-mode). Other features of I-mode include compatibility with low Z impurity seeding to limit power fluxes to the all metal (tungsten and molybdenum) divertor surfaces, and a favorable energy confinement scaling with total input power compared to conventional H-modes. I-mode could prove to be an attractive alternative to the conventional H-mode for ITER.

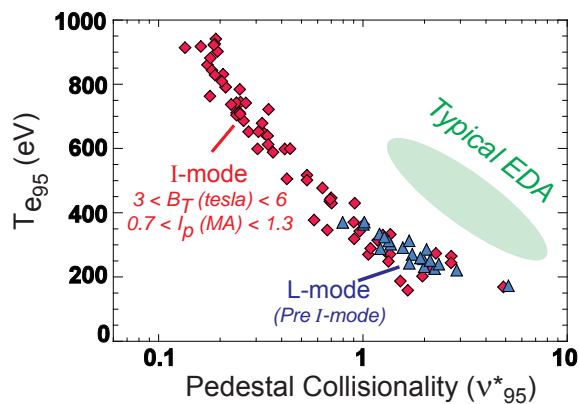


Fig 2.2. Pedestal temperatures and collisionalities for I-mode and L-mode discharges. Typical ranges for EDA H-modes are also shown.

Low Z impurity seeding has also resulted in significantly improved high power performance of the ICRF antennas, with routine fault-free operation achieved in both I- and H-modes for coupled power densities up to 11 MW/m² at the antenna-plasma interface. With seeding, antenna loading is not affected; however, the power outflux from the plasma to outboard limiters and the

antennas is substantially reduced, and the resulting elimination of antenna hot spots is the leading candidate to explain the improved performance.

3. Intrinsic Rotation

Rotation and velocity shear play important roles in the suppression of deleterious MHD modes [3.1] and turbulence [3.2] in tokamak plasmas. Rotation is normally driven by neutral beam injection, but this method may not be effective in future devices. An alternative approach is to take advantage of self-driven flows, the intrinsic rotation which has been widely observed in plasmas without external momentum input [3.3]. A fundamental

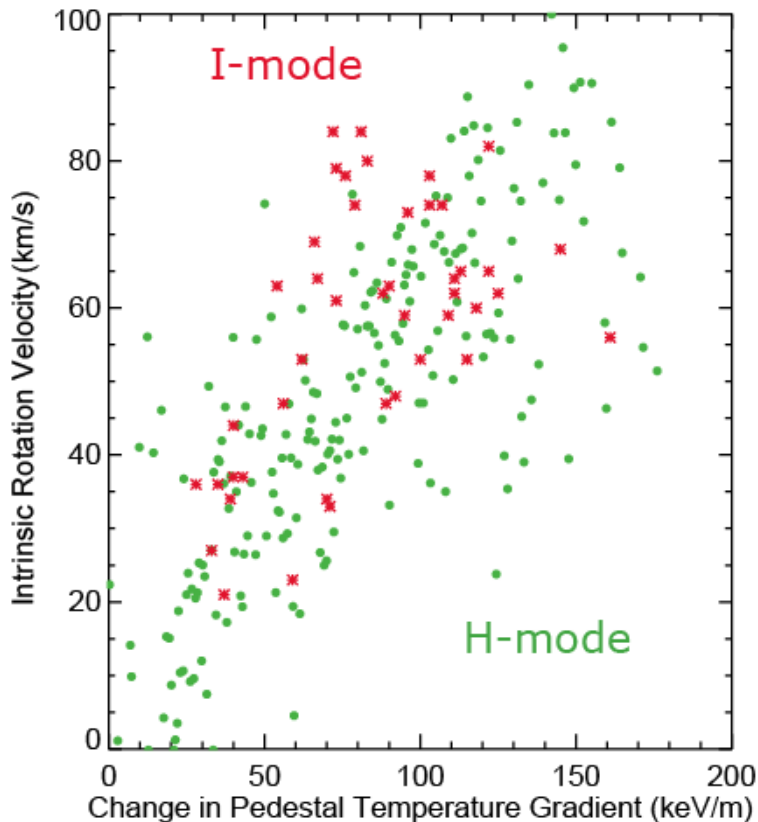


Figure 3.1: The change in the core toroidal rotation from L-mode to I-mode (red asterisks) and to H-mode (green dots) as a function of the change in the pedestal temperature gradient.

understanding of this curious phenomenon is necessary in order to extrapolate confidently to reactors. The mechanism responsible for spinning up the plasma from rest is thought to be the turbulent driven residual stress [3.4]. The core intrinsic toroidal rotation has been found to be well correlated with the plasma stored energy in H-mode plasmas in Alcator C-Mod [3.5] and many other devices [3.3]. For H-mode plasmas, it has been established in C-Mod that the intrinsic rotation originates at the plasma edge, and propagates in to the core on a momentum confinement time scale [3.6]. Similar behavior is seen in I-mode plasmas. Following the transition to I-mode, the rotation velocity first appears at the plasma edge, then propagates in to the plasma center. In the case of I-mode plasmas, the heat and particle transport are decoupled, allowing a unique opportunity for energy barriers to be studied separately; in H-modes both transport channels are usually linked. Since there is no particle barrier in I-mode, the edge pressure gradient is considerably lower (about a factor of three in this comparison) compared to EDA H-mode. The pedestal E_r well depth is also shallower in I-mode compared to H-mode [3.7].

It is well documented that the change in the toroidal rotation velocity between L- and H-mode is proportional to the change in the plasma stored energy [3.5, 3.3]. Similar behavior is

apparent in I-mode as well. This scaling holds over a large range of plasma parameters (density, plasma current, magnetic field, ICRF power). The I-mode results overlay the H-mode points from a large database, suggesting a common phenomenology gives rise to the rotation. Given the evidence that the origin for the intrinsic rotation is in the pedestal region, it is natural to seek a local edge gradient rather than the global stored energy as the rotation drive. Shown in Fig. 3.1 is the change in the rotation velocity as a function of the change in the pedestal electron temperature gradient. (In these C-Mod plasmas, the edge ion and electron temperatures are the same [3.7].) The I-mode results break the correlation with edge pressure gradient, strongly pointing to temperature gradient as the dominant drive for the intrinsic rotation.

4. ICRF Mode-Conversion Flow Drive

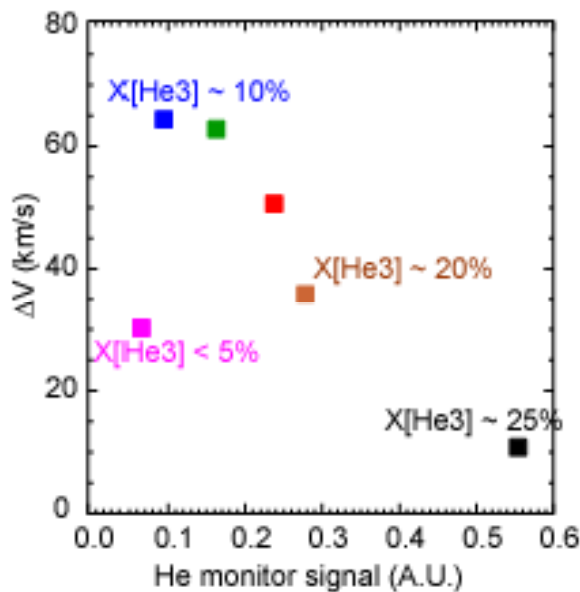


Fig. 4.1. Change of central toroidal rotation velocity vs ^3He emission intensity. The concentrations are derived from Phase Contrast imaging measurements of the mode conversion locations.

Unlike the intrinsic rotation in L-mode, no dependence has been found on plasma topology (upper-null vs. lower-null). At +90° antenna phase (waves in co- I_p direction) and dipole phase (waves symmetrical in both directions), we find that ΔV in the co- I_p direction is proportional to the RF power, and also increases with I_p (opposite to the $1/I_p$ intrinsic rotation scaling in H-mode). The flow drive efficiency is also higher at lower antenna frequency. A maximum central $\Delta V \sim 110$ km/s at 2.7 MW PRF in L-mode has been achieved. Results in H-mode follow the same parametric scaling. However, the observed ΔV in H-mode has so far been

ICRF mode conversion flow drive (MCFD) [4.1] may be a candidate for the external control of plasma rotation in large tokamaks like ITER. Recently, we have carried out a detailed study of MCFD on the Alcator C-Mod tokamak, including its dependence on plasma and RF parameters. These results shed some light on the underlying physics and can help to extrapolate the method to other fusion devices. As seen in figure 4.1, the flow drive efficiency is found to depend strongly on the ^3He concentration in D(^3He) plasmas, a key parameter separating the minority heating and mode conversion regimes. This result further supports the key role of mode conversion. The flow drive efficiency is also strongly affected by plasma density ($\sim 1/n_e$), that is, a power and/or momentum per particle dependence.

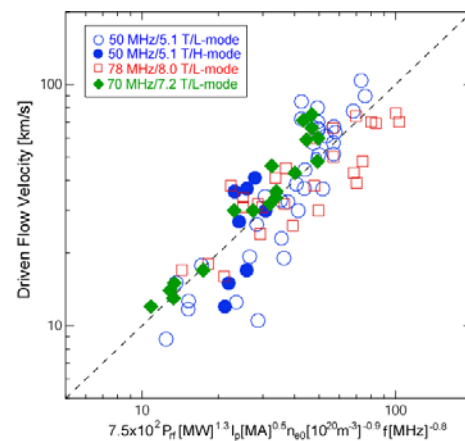


Fig. 4.2. Empirical scaling law for driven flow from 180° and +90° (co-current) antenna phasing.

small, because of the much higher density and the unfavorable $1/n_e$ scaling. As shown in figure 4.2, an empirical scaling law for $+90^\circ$ phasing and 180° phasing has been obtained. On the other hand, the behavior at -90° antenna phase is more complicated. At low RF power, ΔV at -90° phase is similar to the other phases, but at high I_p and high power, the flow drive effect appears to be saturated (and to decrease) vs. RF power. This observation indicates that possibly two mechanisms are involved in determining the total torque: one is RF power dependent, which generates a torque in the co- I_p direction, and the other is wave momentum dependent, i.e., the torque changes direction as a function of antenna phasing.

5. Lower Hybrid Current Drive

Lower Hybrid Current Drive (LHCD) experiments on C-Mod have shown efficient current drive in single null L-mode discharges up to line averaged electron densities of $\sim 1 \times 10^{20} \text{ m}^{-3}$. Hard x-rays (HXR) and relativistic downshifted electron cyclotron emission (ECE) from the LH driven non-thermal electrons, and thus also the LH driven current, drop dramatically above this density limit (see Fig. 5.1) [5.1]. This limit occurs at a density lower than expected based on results from LHCD experiments on limited tokamaks [5.2, 5.3]. Adding a scrape off layer (SOL) model with collisional absorption to the ray tracing/Fokker-Planck model greatly improves agreement between the experiment and simulation.

Scans of plasma topology and position show that non-thermal emission can be enhanced at high density. Operating in balanced double null configuration increases HXR emission slightly, while limited discharges show a significant increase in HXR emission (see Fig. 5.2a) [5.4]. Fueling location (high field side vs. low field side) may also play a small but important role. Decreasing the plasma—inner wall gap also increases HXR emission at high density, with the strongest HXR emission with zero gap (see Fig. 5.2b).

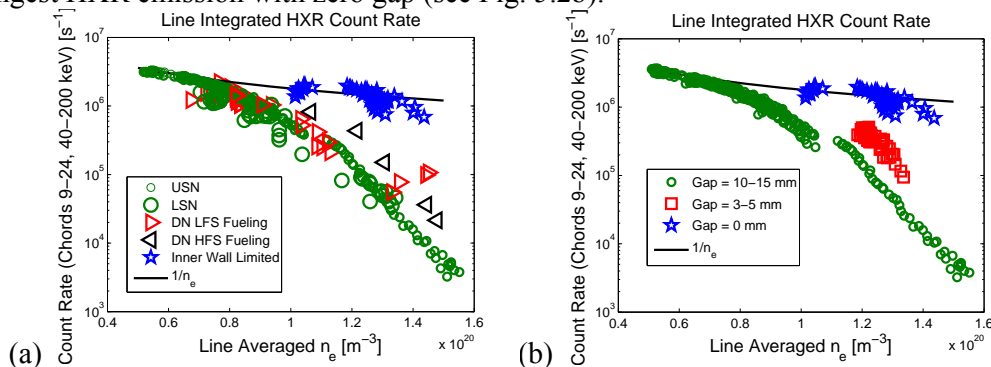


Fig 5.2. (a) HXR emission as a function of plasma topology. (b) HXR emission as a function of plasma—inner wall gap.

Increasing plasma temperature in the plasma edge ($r/a > 0.8$) has been shown to improve LHCD efficiency at high density in a limited tokamak (FTU) by inhibiting parametric instabilities [5.5]. When LHCD is applied to I-mode discharges on C-Mod, which have an H-mode like temperature pedestal with no density pedestal, the non-thermal emission increases

at high density, although the effect is not as pronounced as the change from diverted to limited configuration. Thus, increasing edge temperature does not appear to eliminate the LHCD density limit in diverted tokamaks.

6. Disruption Mitigation

Disruption mitigation is a crucial issue for ITER[6.1]. Viable techniques for reducing halo current forces and thermal loads have been successfully developed and tested on a number of tokamaks[6.2-6.4]. However, avalanche growth of very high-energy (multi-MeV) populations of electrons (up to 10 MA) in ITER is a disruption-related critical issue for which viable mitigation techniques have not yet been developed. Alcator C-Mod's lower hybrid

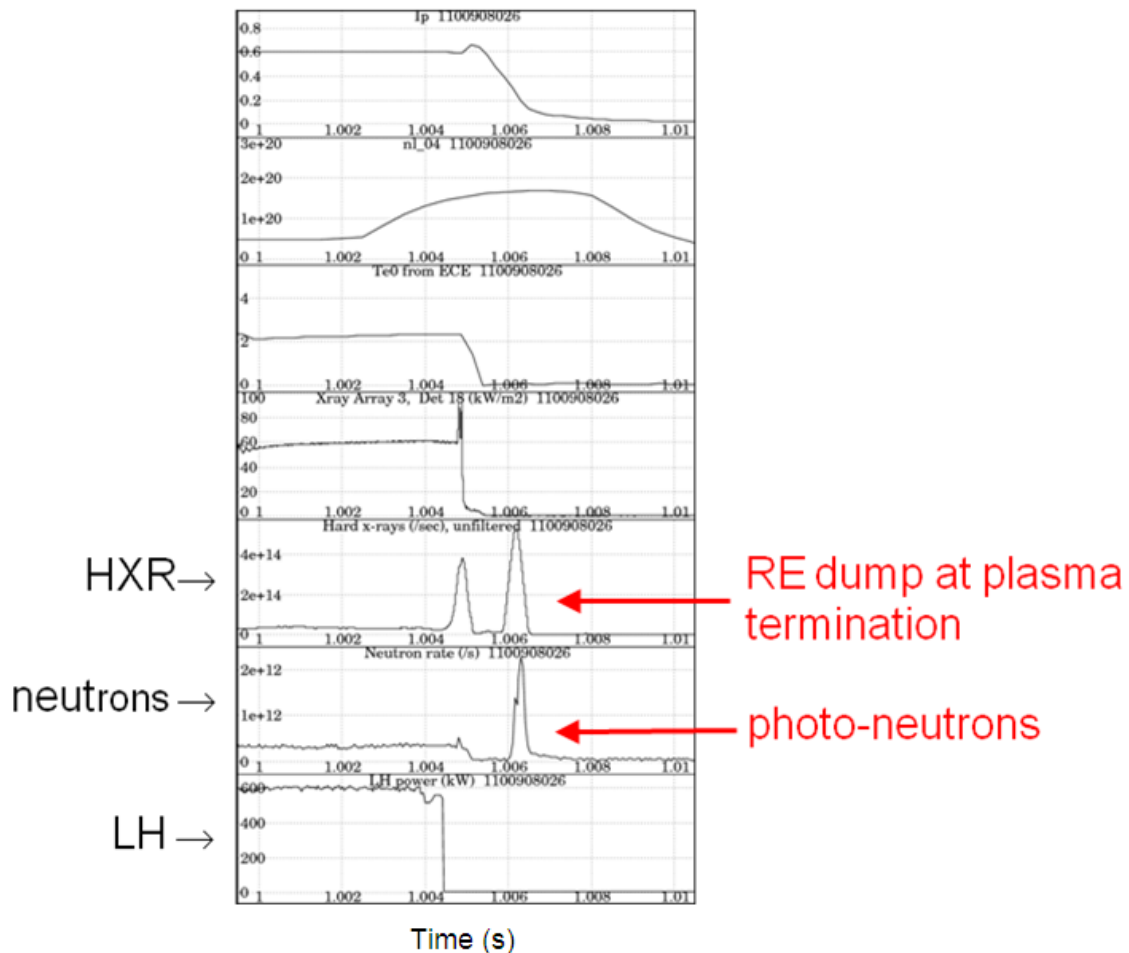


Fig. 6.1. Time history of plasma parameters during a massive gas-puff mitigated disruption seeded with epithermal electrons due to lower hybrid current drive. In this low elongation, inner-wall limited plasma, there is a dump of non-thermal electrons at the thermal quench, and a second dump, of higher energy electrons, during the current quench.

current drive (LHCD) system is an ideal tool for generating large numbers of suprathreshold electrons (~ 50 - 200 keV), which can provide a seed population for studying disruption runaway physics using a number of relevant diagnostics, such as an array of hard x-ray energy analyzers and synchrotron-imaging cameras, as well as other key tools such as the gas jet

disruption mitigation system. The goal is to gain understanding of runaway electron (RE) growth, confinement, and loss mechanisms, and eventually the development of practical runaway electron mitigation techniques. In the initial C-Mod LHCD disruption runaway experiments on standard-elongation, diverted equilibria, no detectable RE's were observed in the disruption current quench (CQ), even though LHCD-driven suprathermals were carrying 10-50% of the pre-disruption plasma current, implying that all of the fast electrons were being lost at the thermal quench (TQ). This was in stark contrast to many other tokamaks, nearly all of which operated with much lower elongation (mostly circular), limited configurations for the studies. MHD modeling of the C-Mod disruptions [6.5] using the 3-D NIMROD code showed that strong MHD activity is triggered by the gas jet injection, resulting in stochastic field regions covering nearly all of the plasma cross-section, and subsequently leading to complete loss of the fast electron seed at the TQ. Recently these disruption runaway experiments have been repeated on C-Mod using low-elongation, limited configurations. As seen figure 6.1, in these discharges, a burst of energetic hard x-rays and photo-neutrons occurs at the end of the CQ when the plasma extinguishes on the inboard wall, although no modification of the plasma current evolution is observed, nor any forward-concentrated visible emission. This implies that a small, but finite fraction of the LHCD suprathermal seed survives through the TQ and gets accelerated during the CQ to energies of at least 10 MeV. This acceleration is consistent with the observed disruption loop voltage and CQ timescale. During the time between the TQ and the RE dump at the end of the CQ, few, if any hard x-rays or photo-neutrons are observed, indicating that the relativistic electrons are well-confined during the CQ. This may imply that flux surfaces in C-Mod re-heal after the TQ, and that RE knock-on avalanche growth should be occurring. The lack of a plateau in the plasma current evolution during the CQ is not necessarily inconsistent with avalanche growth, since during the ~ 1 ms duration of the CQ there should only be a few e-foldings of growth of the RE population. A rough estimate of the current carried by the relativistic RE's during these discharges can be made by comparing the number of photo-neutrons in the dump to that in one of the extremely rare slideaway shots in C-Mod, in which most or all of the plasma current may be carried by RE's. Such a comparison leads to an order-of-magnitude estimate of 100 amperes in these LHCD-seeded disruption runaway discharges. The duration of the CQ is limited by the relatively slow response of the vertical field power supplies, resulting in the termination of the plasma on the inboard wall. We are currently investigating whether appropriate pre-programming of the relevant power supplies might possibly extend the CQ for several more milliseconds, which would allow avalanching up to observable levels on the current evolution.

7. Hydrogenic Isotope Retention

A recent study of D retention in Alcator C-Mod [7.1] found that retention in molybdenum and tungsten PFC surfaces during single, non-disruptive discharges, was 1-2% of the incident fluence to divertor plates, not saturating over sequential discharges. In contrast, post-campaign analysis of an outer divertor tile gave retention fractions that were negligible compared to that for a single discharge (1000x lower). As a possible explanation of this large difference it was shown that the D^0 released in disruptions (occurring in 15% of all discharges), on average, was the equivalent to that retained in 6-7 non-disruptive discharges, thus giving a rough balance over the run period.

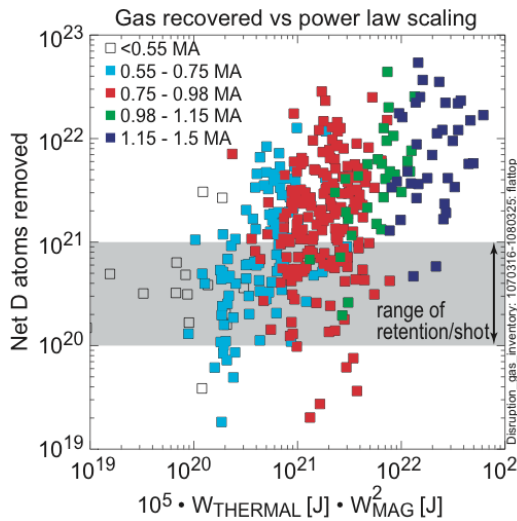


Fig. 7.1: Fuel recovered in disruptions vs the scaling derived from the data. $W_{MAGNETIC}$ is the total poloidal magnetic energy. The range of retention shown corresponds to 1% of ion fluence to PFCs.

big factor is how much of that plasma energy reaches the surrounding surfaces as radiation (heating the entire chamber) versus being carried by plasma to wetted PFCs (concentrated), the latter being much more effective at surface heating.

Given that disruptions lead to such high levels of fuel recovery in C-Mod we have explored what levels (magnetic and thermal stored energy) of disruptions would lead to the same level of temperature rises in an all-tungsten ITER divertor - thus opening the possibility of using low plasma energy disruptions of L-mode ITER plasmas for tritium recovery. We have found that 73 MW, along with of order 6-7 MA, is required in ITER to achieve the same temperature rise as a fairly robust C-Mod discharge ($W_{TH} = 150$ kJ, $I_p = 1.5$ MA). The applicability of such an approach to ITER is uncertain given the results from JET being much less optimistic in terms of fuel recovered. However, when JET compared C-dominated to Be-dominated plasma disruptions [7.5] Be-dominated plasmas led to lower radiation in disruptions which would be consistent with the relatively high levels of plasma flow directly to the wetted PFCs in C-Mod.

8. Radiative H-modes with Low-Z Seeding

Power requirements for maintaining suitably high confinement (i.e., normalized energy confinement time $H_{98} \geq 1$) in H-mode and its relation to H-mode threshold power, P_{th} , [8.1] are of critical importance to ITER. In order to better characterize these power requirements and to complement prior examinations on JET[8.2], recent experiments on the Alcator C-Mod tokamak have investigated H-mode properties, including the edge pedestal and global confinement, over a range of input powers near and above P_{th} . In addition, we have examined the compatibility of impurity seeding with high performance operation, and the influence of plasma radiation and its spatial distribution on performance. Experiments were performed at

More recently [7.2], the fuel recovered in one run period's disruptions was fit to a model of the form $An_e^\alpha I_p^\beta W_{TH}^\gamma$ where the pre-disruptive values of density (n_e), plasma current (I_p) and plasma thermal energy (W_{TH}) are the dependent variables. There was no dependence on density. Figure 7.1 displays the fuel recovered vs the prediction of the regression where we have substituted the total poloidal magnetic energy which is proportional to the square of the plasma current, $0.5LI_p^2$. Figure 2 shows that the amount of fuel recovered can be 30-50x that retained in a single, non-disruptive discharge. This is in contrast to that obtained on other machines where the fuel recovered is roughly the same as that retained in a single discharge [7.3,7.4]. The large scatter in the data are likely due to prior history (initial surface temperature, conditioning and disruptions) as well as the specific surface heated by the disruption. Since the stored energy is converted to plasma energy in a disruption a

5.4T at ITER relevant densities, utilizing bulk metal plasma facing surfaces and ion cyclotron range of frequencies waves for auxiliary heating. Input power was scanned both in stationary enhanced D_α (EDA) H-modes with no large ELMs and in ELMy H-modes in order to relate the resulting pedestal and confinement to the amount of power flowing into the scrape-off layer, P_{net} , and also to the divertor targets. In both EDA and ELMy H-mode, energy confinement is generally good, with H_{98} near unity. As P_{net} is reduced to levels approaching that in L-mode, pedestal temperature diminishes significantly and normalized confinement time drops. This is shown in figure 8.1(a), using both seeded and unseeded discharges. Through seeding with low-Z impurities such as Ne and N_2 , high total radiated power fractions

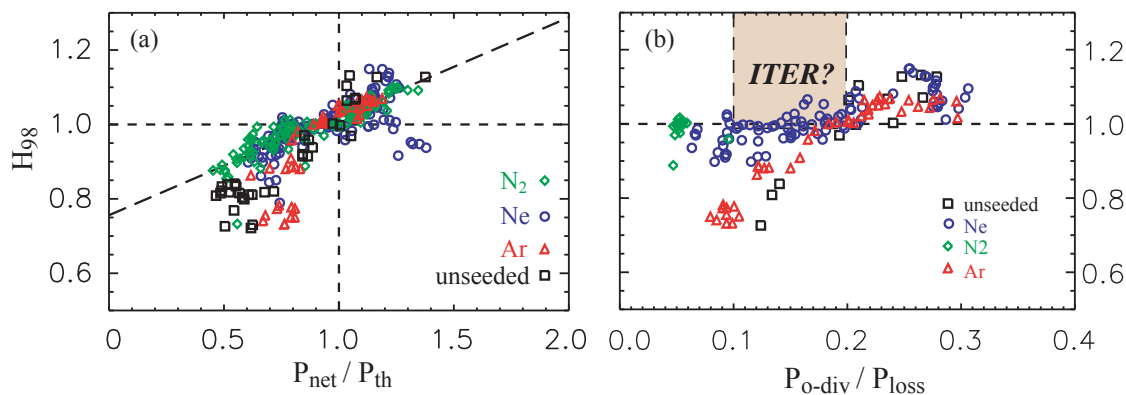


Fig 8.1. (a) Confinement in EDA H-modes with intrinsic impurity content only (black) and seeded with Ar, Ne and N_2 , as a function of $P_{\text{net}}/P_{\text{th}}$. (b) H_{98} vs. the fraction of loss power falling on the outer divertor. A critical question is whether ITER can operate within the pink box.

are possible ($P_{\text{rad}}/P_{\text{in}} \sim 0.7$), along with substantial reductions in divertor heat flux ($>4x$), all while maintaining $H_{98} \sim 1$, as seen in Figure 8.1(b).

When the power radiated from the confined vs. unconfined plasma is examined, pedestal and confinement properties are clearly seen to be an increasing function of P_{net} , helping to unify the results with those from unseeded H-modes. This provides increased confidence that the power flow across the separatrix is the correct physics basis for extrapolation to ITER. The experiments show that $P_{\text{net}}/P_{\text{th}}$ of one or greater is likely to lead to $H_{98} \sim 1$ operation, and also that such a condition can be made compatible with a low-Z radiative impurity solution for reducing divertor heat loads to levels acceptable for ITER.

9. Planned upgrades and future directions

Significant facility and diagnostic upgrades are planned for implementation over the next two years. A new, magnetic-field aligned ICRF antenna will be utilized to test ICRF sheath physics and impurity generation. Additional microwave source power at 4.6 GHz, combined with a second advanced grill, will bring the total complement of Lower Hybrid Current Drive power to 4 MW source (~ 2.5 MW launched) aimed at fully non-inductive advanced scenario studies. A new high-z outer divertor, with active temperature controlled, is designed to test recycling and retention physics at DEMO-relevant plasma-facing component temperatures. Planned diagnostic enhancements include an accelerator-based in-situ first wall surface analysis facility, ECE temperature fluctuation diagnostic, Doppler reflectometry, a new SOL Thomson scattering system, and significant upgrades to existing reflectometer, polarimeter, and MSE systems.

10. References

- [1.1] MARMAR, E.S. et al., Nucl. Fusion 49 (2009) 104014.
- [2.1] WHYTE, D.G. et al., Nucl. Fusion 50(2010)105005.
- [3.1] STRAIT, E.J. et al., Phys. Rev. Lett. 74 (1994) 2483.
- [3.2] HAHM, T.S. Phys. Plasmas 1 (1994) 2940.
- [3.3] RICE, J.E. et al., Nucl. Fusion 47 (2007) 1618.
- [3.4] DIAMOND, P.H., et al., Nucl. Fusion 49 (2009) 045002.
- [3.5] RICE, J.E., et al., Nucl. Fusion 39 (1999) 1175.
- [3.6] LEE, W.D. et al., Phys. Rev. Lett. 91 (2003) 205003.
- [3.7] MCDERMOTT, R.M. et al., Phys. Plasmas 16 (2009) 056103.
- [4.1] LIN, Y. et al., Phys. Rev. Lett. 101 (2008) 235002.
- [5.1] WALLACE, G. M. et al., Physics of Plasmas **17** (2010) 082508.
- [5.2] PORKOLAB, M. et al., Physical Review Letters **53** (1984) 450.
- [5.3] PERICOLI-RIDOLFINI, V. et al., Physical Review Letters **82** (1999) 93.
- [5.4] WALLACE, G. M. et al., this conference (2010).
- [5.5] CESARIO, R. et al., Nat. Commun. **1** (2010) 55.
- [6.1] SUGIHARA, M. et al., Proc. of 20th IAEA Fusion Energy Conference (2004).
- [6.2] MAST, F., J. Nucl. Materials 290-293 (2001) 1045.
- [6.3] WHYTE, D.G., et al., Phys. Rev. Lett. 89 (2002) 055001.
- [6.4] GRANETZ, R.S. et al., Nucl. Fusion 47 (2007) 1086.
- [6.5] IZZO, V.A. Nucl. Fusion 46 (2006) 541.
- [7.1] LIPSCHULTZ, B. et al., Nucl. Fusion 49 (2009) 045009.
- [7.2] LIPSCHULTZ, B. et al., J. Nucl. Materials (2010) in press.
- [7.3] PHILIPPS, V. et al., J. Nucl. Materials 390-391 (2009) 1.
- [7.4] PEGOURIE, B. et al., J. Nucl. Materials (2010) in press.
- [7.5] HARRIS, G., Comparisons of current decay during carbon-bounded and beryllium-bounded disruptions in JET, JET R-90/07 (1990).
- [8.1] MARTIN, Y.R. et al. Journal of Physics: Conference Series **123** (2008) 012033.
- [8.2] SARTORI, R. et al. Plasma Phys. Control. Fusion **46** (2004) 723.

This work is supported by U.S. Department of Energy Office of Fusion Energy Sciences.